 doi:10.20944/preprints202104.0164.v1

Type of the Paper (Article)

A two-fluid model for high viscosity upward annular flow in vertical pipes

Joseph X. F. Ribeiro [1,2,3]*, Ruiquan Liao [1,2], Aliyu M. Aliyu [4], Salem K. B. Ahmed [5], Yahaya D. Baba[6], Almabrok A. Almabrok[7], Archibong Archibong-Eso[8] and Zilong Liu [1,2]

1 Petroleum Engineering College, Yangtze University, 430100, Wuhan, Hubei, China. : joseph.xfribeiro@kstu.edu.gh, liaoruiquan@263.net, 329165325@qq.com
2 Laboratory of Multiphase Flow, Gas Lift Innovation Centre, China National Petroleum Corporation
3 Kumasi Technical University, P. O. Box 854, Kumasi, Ghana; joseph.xfribeiro@kstu.edu.gh, liaoruiquan@263.net, 329165325@qq.com
4 School of Computing and Engineering, University of Huddersfield, HD1 3DH, United Kingdom; a.m.aliyu@hud.ac.uk
5 Faculty of Mining and Energy Engineering, Sebha University, Lybia; Sal.brini@sebhau.edu.ly
6 Department of Chemical and Biological Engineering, University of Sheffield, Sheffield S1 3JD, UK; y.baba@sheffield.ac.uk
7 Department of Petroleum Engineering, Faculty of Engineering, Sirte University, Sirte, Lybia; almabrok.abushanaf@su.edu.ly
8 Department of Mechanical Engineering, University of Birmingham, Dubai International Academic City, Dubai; a.e.archibong@bham.ac.uk
* Correspondence: joseph.xfribeiro@kstu.edu.gh; joxaro@yahoo.com ; Tel.:+23324446160

Abstract: Selection of appropriate friction factors is paramount for accurate prediction of key flow characteristics in gas–liquid two-phase flows. In this work, experimental investigation of vertical air and oil (with viscosities up to 200 mPa s) flow in a 0.060-m ID pipe is reported. Superficial air and oil velocity ranges utilized are from 22.37 to 59.06 m/s and 0.05 to 0.16 m/s respectively. The influence of estimation of interfacial friction factor on accurate determination of film thickness, void fraction and pressure gradient was investigated using a two-fluid model. The results indicated that the two-fluid model is capable of accurately predicting flow characteristics. Further, it reveals that the best performing correlations are the Belt et al. and Ambrosini et al. correlations.

Keywords: two-phase flow; interfacial friction factor; vertical pipes, higher viscosity, pressure drop

1. Introduction

Two-phase gas-liquid upward annular flow plays a key role in numerous industrial applications. Flow of refrigerants in air-conditioning and refrigeration systems, transportation of oil and gas products in petroleum industries and steam in power plants as well as nuclear reactor core cooling constitute a few examples of such applications. Among the most prominent two-phase flow regimes in many of these applications is annular flow.

Annular flow in pipes is generally characterized by a thin liquid film flowing along the pipe periphery with gas flow in the core region. Its practical importance to industry coupled with the comparative ease with which it lends itself to analytical deductions has made this flow regime the focus of extensive investigations both experimentally and analytically [1].

One major objective which provides thrust for multiphase flow research is gaining insight into the impact of operating factors on flow characteristics including velocity distribution, liquid film thickness, gas void fraction (liquid holdup) and pressure gradient. The one-dimensional two-fluid model has often been employed by several authors for such investigations. For turbulent two-phase flows, the one- dimensional modeling of annular flow is recognized as a practical tool for the analysis of essential flow character-

 doi:10.20944/preprints202104.0164.v1

istics including liquid holdup and pressure drop (pressure gradient). However, the various treatments available in the open literature are limited to air–water flows, or with liquids of near-water viscosities. In many industrial applications such as food and cosmetics, viscous slurries are processed as well as in oil and gas where heavy oil processing and transport is becoming more prevalent. It is therefore necessary to study the performance of models, particularly the 1D two-fluid in predicting key flow parameters.

1.2 Previous works

Previous research has utilized the two-fluid model in attempts to predict some flow characteristics [2]–[6]. Based on the Harwell databank, Oliemans et al. [3] developed correlations for interfacial friction factor and liquid entrainment fraction. These correlations were further employed in a two-fluid model for prediction of pressure loss, liquid film thickness and liquid entrainment in annular dispersed flow. Reported results indicated good agreement with the experimental data. Alves et al [2] employed the two-fluid model to predict the aforementioned flow characteristics. The model was found to accurately predict the experimental data and performed better than existing models including that of Aziz et al.[7] among others [8]–[12]. Zhang et al. [6] employed a two-fluid approach to develop a unified mechanistic model capable of predicting flow pattern transitions, pressure gradient, liquid holdup and slug characteristics in the gas-liquid pipe flow all angles of inclination. Using oils of viscosity 10 and 12 mPa s respectively as the liquid phase and air as the gas phase, Alamu [4] compared his annular flow data with predictions Alves et al. [2] two- fluid model. Good agreement was found between the measured parameters and prediction of the model. As part of their experimental study, Vieira et al. [5] utilized the two-fluid mechanistic model of Shoham to examine void fraction data (obtained using liquid viscosities of 1, 10 and 40 mPa s respectively, pipe diameter of 0.076 m). Though the authors observed that predictions of the model capture the trend, they reported that the model overpredicted the gas void fraction experimental data.

From the discussion of previous studies, it has been demonstrated that majority of reported studies, which have employed the two-fluid model, have been carried out using liquids of low viscosities. Variations in liquid viscosity influences flow characteristics. Insight into behavior of such liquids is critical for both research and equipment design [5], [13]. In this study, the reliability of the two-fluid approach is investigated with respect to liquid film thickness, gas void fraction, and pressure gradient using higher viscosity liquids and a 60-mm ID pipe for the annular flow regime in vertical pipes. The solution of the hydrodynamic model considers the momentum of the gas and liquid phases to present a complete solution for the interface configuration and associated flow characteristics for a variety of experimental conditions. While the two-fluid model is mechanistic, closure relationships are often empirical in nature. The limitations of the empirical correlations can significantly impact the accuracy of predictions of liquid holdup and pressure gradient. Also, in this study, the validity of the model and its practical significance for analyzing the annular flow configuration and the related pressure drop on a gas-liquid system is investigated. Further, the impact of selected closure relationships on estimation of liquid film thickness, gas void fraction and pressure gradient are examined. This is achieved by comparing predictions of the two-fluid model with experimental data.

1.3 The two-fluid model

Figure 1 illustrates the annular flow regime in a vertical pipe. It also highlights the control volume used for the momentum balance derived for this study.

Preprints (www.preprints.org) | NOT PEER-REVIEWED | Posted: 6 April 2021 doi:10.20944/preprints202104.0164.v1

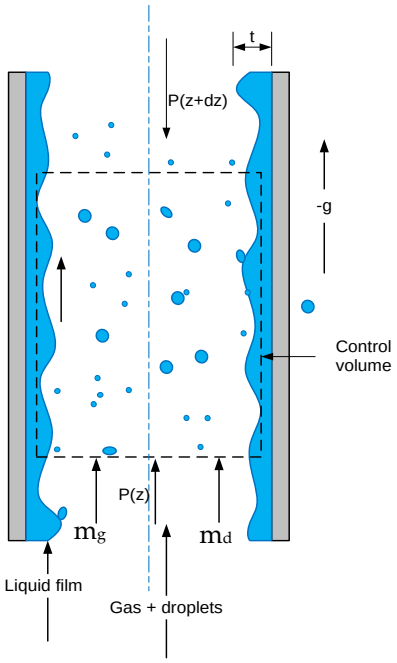

Figure 1. Control volume for the momentum balance in Eq. (14) (Wongwises and Kongkiatwanitch, 2001; Aliyu et al., 2017)

The momentum (force) balances for the liquid film and core are given by Equations (1) and (2) respectively as follows:

$$-\tau_{wL}\frac{S_L}{A_F}+\tau_i\frac{S_I}{A_F}-\left(\frac{dp}{dL}\right)_F-\rho_l g\sin\theta=0 \tag{1}$$

$$\tau_i\frac{S_I}{A_C}-\left(\frac{dp}{dL}\right)_C-\rho_c g\sin\theta=0 \tag{2}$$

For fully developed flow at steady state, pressure gradient in the film and core are deemed equal. Therefore, Equations (1) and (2) can be combined by eliminating the pressure gradient. This results in the combined momentum equation for annular flow, is therefore expressed by:

$$-\tau_{wL}\frac{S_L}{A_F}+\tau_i S_I\left(\frac{1}{A_F}+\frac{1}{A_C}\right)-(\rho_l-\rho_c)g\sin\theta=0 \tag{3}$$

For upward annular flows in vertical pipes, the assumption of uniform film thickness around the pipe is valid. The geometrical parameters, therefore, can be derived based on a uniform film thickness, δ_l as follows:

$$A_C=\pi(d-2\delta_l)^2/4 \tag{4}$$

$$A_F=\pi\delta_l(d-2\delta_l) \tag{5}$$

$$S_I=\pi(d-2\delta_l) \tag{6}$$

$$S_L=\pi d \tag{7}$$

Preprints (www.preprints.org) | NOT PEER-REVIEWED | Posted: 6 April 2021 doi:10.20944/preprints202104.0164.v1

$$v_F = v_{sl}\frac{(1-f_E)d^2}{4\delta_l(d-\delta_l)} \tag{8}$$

$$v_C = \frac{(v_{sg}+v_{sl}f_E)d^2}{(d-2\delta_l)^2} \tag{9}$$

The liquid friction factor f_L is calculated using the Blasius equation based on the film Reynolds number, Re_F, which considers the hydraulic diameter as the ratio of four times the area of the wetted perimeter, given by:

$$Re_F = \frac{\rho_l v_F}{\mu_l}\frac{4\delta_l(d-\delta_l)}{d} \tag{10}$$

If $Re_F < 2100$, $f_g = 16$, $n = 1$

Else $f_g = 0.046$, $n = 0.2$

$$f_L = f_g Re_F^{-n} \tag{11}$$

$$Re_C = \frac{\rho_C v_C(d-\delta_l)}{\mu_g} \tag{12}$$

Since the main objective of this study is to assess the impact of interfacial friction factors, f_i on the accuracy of predictions of liquid film thickness, gas void fraction and pressure gradient, selected reported f_i correlations are integrated into the solution.

The shear stress occurring between the liquid and the wall is calculated using Eq. 13:

$$\tau_{wL} = f_L\frac{\rho_l(v_F)^2}{2} = f_L\frac{\rho_l\left(v_{sl}\frac{(1-f_E)d^2}{4\delta_l(d-\delta_l)}\right)^2}{2} \tag{13}$$

The interfacial friction factor can be determined by utilizing the following expression (Eq. 14):

$$\tau_i = f_i\frac{\rho_C(v_C-v_F)^2}{2} \tag{14}$$

Substituting Eq. (4) - (7) into Eq. (3), Eq. (15) is obtained as follows:

$$-\tau_{wL}\frac{\pi d}{(\pi\delta_l(d-2\delta_l))} + \tau_i(\pi(d-2\delta_l))\left(\frac{1}{(\pi\delta_l(d-2\delta_l))} + \frac{1}{(\pi(d-2\delta_l)^2/4)}\right) - (\rho_l-\rho_C)g\sin\theta = 0 \tag{15}$$

When a solution is attained for Equation 15, the gas void fraction can be determined using Equation 16 as follows:

Preprints (www.preprints.org) | NOT PEER-REVIEWED | Posted: 6 April 2021 doi:10.20944/preprints202104.0164.v1

$$\alpha_T = \alpha_C \left(1 - 2\frac{\delta_l}{d}\right)^2 \tag{16}$$

Subsequently, the liquid (oil) holdup can be estimated as follows:

$$H_l = 1 - \alpha_T \tag{17}$$

The pressure gradient can then be determined using either Eq. 1 or 2.

1.4 Closure relationships

Selection of closure relationships which couple with the two-fluid model is essential for accurate predictions of flow characteristics [6]. For upward annular flow, key closure relationships required for implementing the two-fluid model include correlations for liquid friction factor, liquid droplet entrainment, and the interfacial friction factor.

In this study, the liquid friction factor f_L is calculated using the Blasius equation based on the film Reynolds number, Re_F, which considers the hydraulic diameter as the ratio of four times the area of the wetted perimeter is used.

Several liquid entrainment correlations have been proposed by several authors [3], [6], [14]–[16]. For this study, however, the Oliemans et al. [3] is utilized. The Oliemans et al. [3] correlation was developed based on the AERE Harwell databank and is expressed as follows:

$$\frac{F_E}{1-F_E} = 10^{\beta_0} \rho_l^{\beta_1} \rho_g^{\beta_2} \mu_l^{\beta_3} \mu_g^{\beta_4} \sigma^{\beta_5} d^{\beta_6} v_{sl}^{\beta_7} v_{sg}^{\beta_8} g^{\beta_9} \tag{18}$$

Values for the indices β_0 to β_9, are presented by the authors and Zhang et al. (2003).

In all, the influence of 9 correlations reported by Ambrosini et al. [17], Akagawa et al. [18], Belt et al. [19], Blasius [20], Fore et al. [21], Holt et al. [22], Moeck (1970), Wallis [14], Wongwises and Kongkiatwanitch [1]are examined for this study. Detailed information of correlations is presented by Aliyu et al. (2017).

The interfacial friction factor correlation proposed by Blasius is mainly applicable to smooth pipes based on a linear approximation between interfacial friction factor and gas Reynolds number [20]. Wallis's correlation for predicting friction factor, one of the most widely used, treats liquid film interface as form of pipe wall roughness and a is function of non-dimensional liquid film thickness [14]. Authors including Moeck [23], Fore et al. [21], Wongwises and Kongkiatwanitch [1] and Belt et al. [19] have also presented Wallis-type correlations which introduce new constants, dimensionless numbers (Reynolds, Froude) and viscosity ratios to account for the effect of liquid viscosity [24]. The f_i correlation presented by Wongwises and Kongkiatwanitch [1] utilize a power law relationship with gas Reynolds number and the non-dimensional film thickness (t/D) as correlating parameters. The Ambrosini et al. [17] correlation is the result of a correlation of interfacial friction factor with Weber number, gas Reynolds number, phase densities and non-dimensional liquid film thickness. The correlation is a refinement of the Asali et al. [25] correlation. Holt et al. [22] modified the Ambrosini et al. [17] correlation being a function of only the Weber and gas Reynolds numbers. The correlation presented by Akagawa et al. [20] is a Wallis-type correlation which is a function of dimensionless liquid film thickness. The correlation was based mainly on air-water upward annular disturbance wave flow data [18]. Belt et al. [19] presented a physical approach to predict the interfacial shear-stress, based on the theory on roughness in single-phase turbulent pipe flows. Their results showed close agreement with the theory. Further, they showed that the assumption that sand-grain roughness of the liquid film is proportional to wave height. They found this assertion more effective compared to the regularly utilized assumption that sand-grain roughness of the liquid film is equivalent to four times the mean film thickness (as suggested by Wallis [14]). Experimental facility description and data processing.

Preprints (www.preprints.org) | NOT PEER-REVIEWED | Posted: 6 April 2021 doi:10.20944/preprints202104.0164.v1

1.5 Test rig description

The experiment was implemented on a test rig capable of inclinations from 0 - 90° (Figure 2) at the Gas Lift Innovation Centre, Yangtze University, China. For each experiment, the desired volume of oil was pumped into a mixing tank, and pressurized. After pressure stabilization and measurement, the liquid is mixed with compressed gas and introduced into the test section. The liquid returns to the mixing tank while the air is released into the atmosphere after the gas-liquid mixture has passed through the separator.

The test section (Figure. 2) is a pipe of length 10.6 m and an ID of 0.060 m. The viewing section consists of an acrylic tube with a length of 7 m. Stainless steel pipes of lengths 1.1 m and 2.5 m respectively are fixed at each end of the acrylic tube. Pressure, temperature, and pressure differential sensors, as well as quick closing valves and other devices are installed on the stainless-steel sections of the pipe. The distance between the two quick closing valves is 9.5 m. The distance between the differential pressure transducers is 8 m. Control of the devices as well as extraction of data is done directly online at the control center. Details of the measuring equipment utilized for the experiment are presented in Table 1. Air constituted the gas phase while oil was used as the liquid phase. The fluid properties used in the experiment are presented in Table 2.

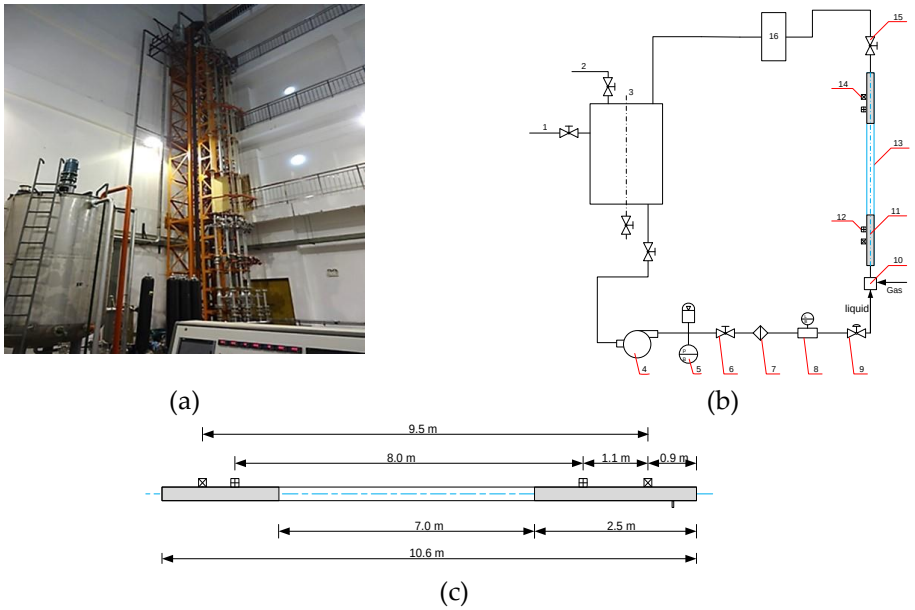

Figure 2. Experimental setup – (a): photo of the experimental rig in vertical position; (b): schematic diagram with numbers denoting (1) Flow Entrance of Oil (2) Flow Entrance of Water (3) Oil-Water Mixer (4) Liquid Pump (5) Pressure Meter (6) Regulator (7) Moisture Content Tester (8) Flow Meter (9) Adjusting Pressure Valve (10) Gas-Liquid Mixer (11) Stainless steel pipe (12) Pressure transducer (13) Acrylic viewing section (14) Quick closing valve (QCV) (15) Valve (16) Gas-Liquid Separator; (c) Dimensions of test section

Table 1: Details of the measuring equipment utilized for the experiment

Equipment	Parameter measured	Measuring range	Measurement error
Rosemount 305 1S Pressure transducers	Pressure	0–3.5 MPa	±0.1%
Endress+Hauser/80E50 Coriolis flowmeter	Liquid Flow Rate	2–20 m^3/h	±0.3%
Endress+Hauser/65F1H Coriolis flowmeter	Gas Flow Rate	160–2000 m^3/h	±0.1%
Limit Switch Box APL-210 quick-closing valves	Liquid holdup	N/A	

Table 2: Fluid properties used in the experiment

Preprints (www.preprints.org) | NOT PEER-REVIEWED | Posted: 6 April 2021 doi:10.20944/preprints202104.0164.v1

Fluid	Gas Air	Liquid Oil
Density (kg/m^3)	1.205	854 (20°C)
Viscosity ($mPa\ s$)	0.0181 (20°C)	100– 330
Surface tension (N/m)	-	0.0287(20°C)

Table 3: Range of experimental data obtained

Superficial liquid velocity (m/s)	**0.05 – 0.16**
Superficial gas velocity (m/s)	22.37 – 59.06
System Pressure (MPa) (gauge pressure)	0.04-0.14
Temperature (°C)	20.99-47.80
Pressure Drop (kPa)	4.62-20.02
Liquid Holdup (-)	0.003-0.269

1.6 Fluid properties for the experiment

Compressed air and white oil constituted the gas and liquid phases, respectively. The oil density was 854 kg/m³ at 20°C with a surface tension of 0.0287 N/m. Variations in density and surface tension of the oil with temperature was small enough to assume it is negligible. Increase in viscosity was achieved by increasing temperature. The behaviour of the oil viscosity versus temperature is as shown in Figure 3.

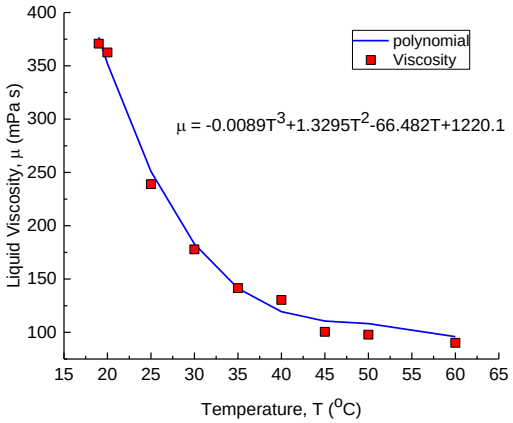

Figure. 3: Variation of oil viscosity with temperature

2. Experimental procedure and measurements

For this experiment, a constant liquid flow rate was maintained, while the gas flow rate is adjusted. When the system was deemed steady (approximately 15 minutes from the start of the experiment), the experimental flow pattern was observed and recorded. Except for liquid holdup, all other experimental data was recorded every 5 seconds for 3 minutes, and finally the average value of each measurement parameter was obtained. Each complete test took approximately 30 minutes depending on the time required to reach steady state. After the data recording was completed, the quick closing valves (2

Preprints (www.preprints.org) | NOT PEER-REVIEWED | Posted: 6 April 2021 doi:10.20944/preprints202104.0164.v1

Limit Switch Box APL-210 mechanical actuators which can be actuated simultaneously with a single switch) were closed trapping fluids flowing in the test section. The quick closing valves have a response time is 0.3–0.5 s. Liquid holdups are measured by using a 9.5 m longitudinal pipe section. liquid into a measuring cylinder. Liquid holdup was estimated by calculating the volume of the liquid and dividing it by the volume of pipe-section. Flow patterns were visualized directly and observed using a Canon Xtra NX4-S1 high-speed camera capable with a pixel resolution of resolution of 1024x1024 up to 3000 frames per second (fps). The maximum frame rate is 50,000 fps with a reduced resolution. Videos and pictures of the flow pattern were obtained and used for analysis during the study. The range of measurements taken during the experiments is presented in Table 3.

Fully developed flow is a key required for multiphase studies. For this experiment, fully developed flow was observed with the camera located at L/D = 133. A survey of similar experiments indicates that fully developed annular flow pattern in vertical pipes have been observed at lower L/D values by a number of researchers including Wongwises and Kongkiatwanitch [1] (L/D = 41), Aliyu et al. [20] (L/D = 46), Fore and Dukler [26] (L/D = 69), Zangana [27] (L/D = 66), Skopich et al. [28](L/D = 59-92), and Van der Meulen [29] (L/D = 87). Shearer and Nedderman [30] conducted some experiments with an L/D = 133. It can be assumed, therefore, that the selected L/D ratio represents a sufficient flow development length.

3. Results

3.1. Experimental results and discussion

3.1.1. Visual Observations and flow regime identification

For all flow conditions in the study, annular flow was observed at all liquid viscosities under consideration. Downward flow of liquid film was not observed at the considered flow conditions. At low phase velocities, a comparatively thick liquid film was observed at all viscosities. The thickness of the liquid film appeared to reduce as gas velocities was increased. Liquid film thickness continued to reduce even when liquid velocity was increased. This was the trend for both viscosities under consideration. Liquid velocities contributed to the total phase momentum driving reduction of the liquid film. This phenomenon is consistent with the findings Fukano and Furukawa [24] who concluded that liquid film thickness decreases independent of liquid viscosity and velocity. Further, at fixed phase velocities, liquid film thickness increased as liquid viscosity increased. It was found that liquid film appeared thicker at 200 mPa s at all superficial velocities (Figure 4).

100 mPa s

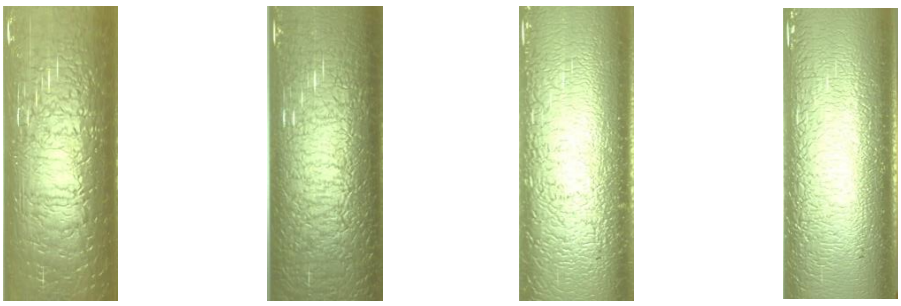

Preprints (www.preprints.org) | NOT PEER-REVIEWED | Posted: 6 April 2021 doi:10.20944/preprints202104.0164.v1

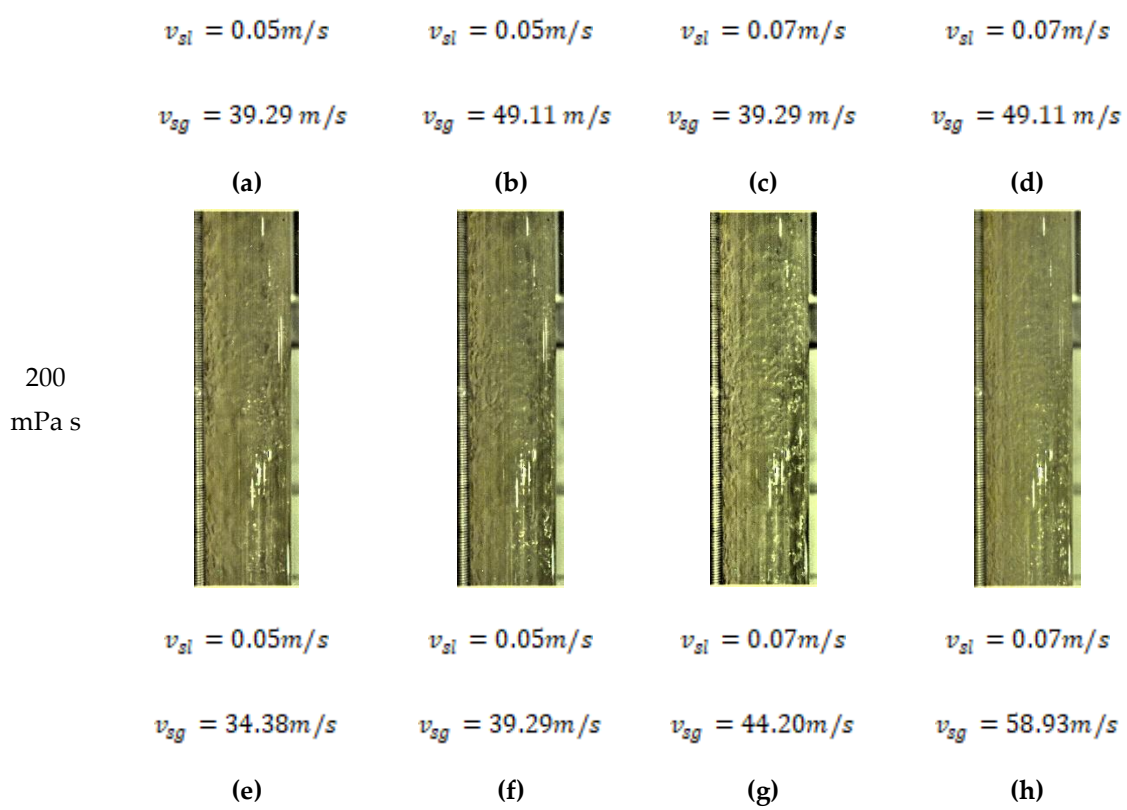

Figure. 4: Flow patterns observed at different v_{sg} values for v_{sl} values of 0.05 and 0.07 m/s for liquid viscosities of 100 and 200 mPa s respectively

Ripples were also observed on the surface of the liquid films at different flow conditions for different liquid viscosities (Figure 4). Ripples appeared to decrease in roughness as gas and liquid velocities increased. The surface of the liquid film appeared comparatively smoother at higher gas velocities. Figure 4 shows ripples on the surface of the liquid film at different superficial phase velocities for liquid viscosities of 100 and 200 mPa s respectively. At 200 mPa s, for instance, it can be observed that ripples exist on the surface of the liquid film at v_{sl} value of 0.05 m/s and v_{sg} values of 34.38 m/s making the surface rough (Figure 4e). At higher superficial gas velocity of, for example 58.93 m/s, comparatively gentle ripples are observed on the surface of the liquid film. Fukano and Furukawa [24] also reported observing ripples on the liquid film surface for all viscosities they considered. They characterized this phenomenon as ripple flow. In addition, the appearance of the wavy surface appeared different for different viscosities even under the same flow conditions. Similar observations were reported by Fukano and Furukawa [24]. The observations agree with their suggestion that interfacial friction factor, which is directly linked to wave characteristics, significantly affected by viscosity.

3.1.2. Visual Observations and flow regime identification

The flow pattern for the various liquid viscosities was observed directly through the acrylic viewing section of the test pipe. Data obtained was superimposed on the Shell flow pattern map (2007) [20], [31] and the flow pattern map of Taitel et al [32] respectively (Figure 5).

Preprints (www.preprints.org) | NOT PEER-REVIEWED | Posted: 6 April 2021 doi:10.20944/preprints202104.0164.v1

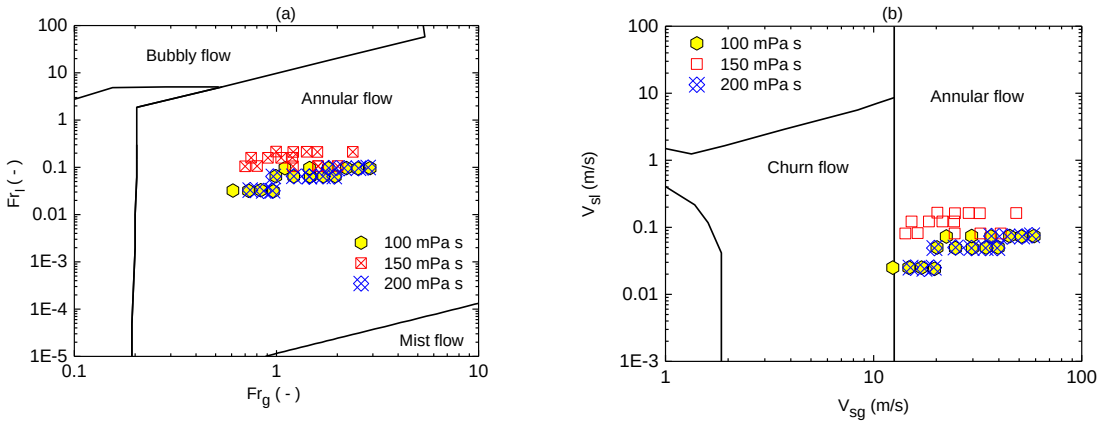

(a) (b)

Figure 5 Experimental data super-imposed on the flow pattern maps of: (a) Shell Company (2007) and (b) Taitel et al. (1980)

Created by the Shell Company [20], [31] for transport (charge and discharge) of combustibles, the Shell map flow pattern map is generalized by using the superficial gas and liquid Froude numbers respectively based on the feed pipe velocity and diameter. For the Shell flow pattern, the densimetric Froude numbers employed are defined as follows:

$$Fr_g = v_{sg}\left(\frac{\rho_g}{(\rho_l-\rho_g)gD}\right)^{0.5} \quad , \quad Fr_l = v_{sl}\left(\frac{\rho_l}{(\rho_l-\rho_g)gD}\right)^{0.5}$$

Though it is observed that the Shell flow pattern map is unable to detect and characterize data points indicating transition to annular flow (Figure 5a), all points are classified as annular flow it is found that the flow pattern map agrees very well with the experimental data. This could be attributed to the closeness of some of the phase properties used in its development (ρ_l = 860 kg/m3, μ_g = 0.00016 Pa.s, and σ = 0.03 N/m) to the experimental fluid properties. Though the flow pattern map was developed with a large diameter (500 mm), this does not seem to provide any limitation.

The Taitel *et al*. [32] flow pattern map was developed by employing different transition criteria which utilized analytical relationships for the force balance between gravity and drag forces acting at the onset of annular flow. The related theories were validated with data obtained from a 50-mm ID pipe. It is found that the flow regime map agrees with the experimental observations.

3.2. Liquid Holdup

Generally, it is observed that at all viscosities, liquid holdup decreases as superficial gas velocity increases as shown in Figure 6. The decrease is sharp at lower superficial gas velocities and asymptotic at higher superficial gas velocities ($v_{sg} > 40\ m/s$) for liquid viscosities of 100, 150 and 200 mPa s respectively. Again, it is found that liquid holdup decreases as superficial liquid velocity increases. However, the decreases do not appear to be significant, especially at higher liquid viscosities. This can be attributed to the fact that increase in quantity and the velocity of the liquid is not enough to counter the effects of the high gas velocity. This makes the contribution of the superficial liquid velocity rather insignificant.

Preprints (www.preprints.org) | NOT PEER-REVIEWED | Posted: 6 April 2021 doi:10.20944/preprints202104.0164.v1

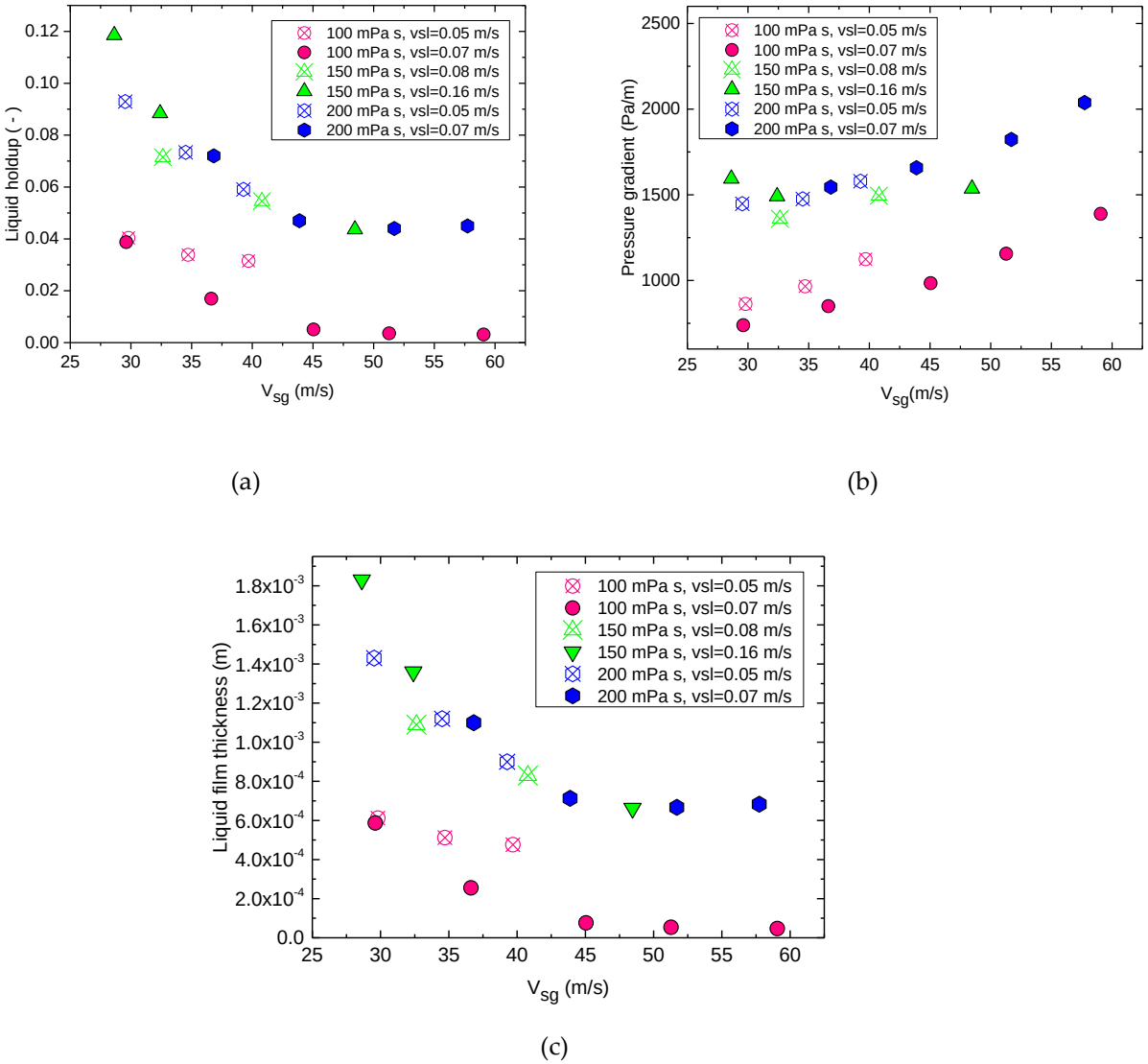

Figure 6 Variation of (a) liquid holdup, (b) pressure gradient and (c) liquid film thickness with superficial gas velocity for liquid viscosities of 100 mPa s, 150 mPa s and 200 mPa s respectively at different v_{sl} values

In addition, the results indicate that at fixed superficial air velocities values, increase in liquid viscosity increases liquid holdup. Increased liquid viscosity results in increased shear stresses which translates into increased liquid accumulation at higher liquid viscosities [33]. Increase in liquid holdup can also be attributed to liquid droplet entrainment behavior with respect to liquid viscosity. Liquid droplet entrainment decreases with increasing liquid viscosity [33].

3.3. Pressure Drop

Pressure drop is found to increase as superficial gas velocity increases. Increasing pressure drop at higher viscosities can be attributed to increase in friction at the gas-liquid interface. The liquid formed at the gas- liquid interface generates an interfacial friction which is normally higher than the gas-wall friction, especially when the gas-liquid interface becomes wavy. Further, increase in pressure drop could be influenced by increments in the density of the gas phase as a result of entrained liquid. Finally, at fixed liquid superficial velocity, as gas superficial velocity increases slip within the gas-liquid interface increases. This phenomenon leads to a higher interfacial shear and corresponding increase in the total pressure gradient [4].

Preprints (www.preprints.org) | NOT PEER-REVIEWED | Posted: 6 April 2021 doi:10.20944/preprints202104.0164.v1

The effect of superficial liquid velocity on pressure drop is not apparent (Figure 6). Perhaps, as earlier explained, the v_{sl} values are too small to make any significant difference. At fixed superficial phase velocities, however, it is found that increase in liquid viscosity increases pressure drop. Increasing liquid viscosity results in increased frictional pressure drop during flow as well as increasing liquid holdup which also translates to increased gravitational pressure gradient. Increases in the two components naturally increases the total pressure drop.

3.4. Liquid film thickness

The variation of liquid film thickness for the liquid viscosities (100 mPa s, 150 mPa s, 200 mPa s) against superficial gas velocity is shown in Fig 7. Results from investigating the behavior of liquid film thickness indicates that it reduces as superficial gas velocity increases. For all superficial liquid velocity values, at all viscosities, liquid film thickness is observed to decrease asymptotically. The decrease is rapid at low superficial gas velocities. Liquid film thickness is maximum at liquid viscosity of 200 mPa s. This is because it presents the greatest resistance to the flow conditions (reducing liquid droplet entrainment and increasing liquid holdup in the process). Liquid film thickness values are highest at liquid viscosity of 200 mPa s and decrease with decreasing liquid viscosity. The observation of the behavior of liquid film thickness when subjected to varied gas velocity is similar to reports by authors who utilized air-water mixtures [1], [20], [34]. Similar findings have also been reported by Fukano and Furukawa [24] and Kaji and Azzopardi [35] who used low viscosity liquids for their experiments.

3.5. Influence of interfacial frication factors on predictions of liquid film thickness, gas void fraction and pressure gradient

For all flow conditions, the combined momentum equation was solved by integrating an interfacial friction factor correlation and comparing liquid film thickness, gas void fraction and pressure gradient predictions for liquid viscosities of 100 and 200 mPa s with experimental data. Here, comparison of the prediction of the targeted flow characteristics is made. The effect of combining the popular liquid friction factor of Blasius with several interfacial friction factors is presented. The Oliemans et al. [3] correlation for liquid entrainment fraction is used for this study.

To solve the combined momentum equation, the MATLAB *fsolve* function was employed. The function fsolve is a non-linear system solver which resolves problems expressed as:

$$F(x) = 0 \tag{19}$$

for x (vector or matrix), where F(x) is a function that returns a vector value. Input values for superficial liquid and gas velocities, liquid viscosity and an initial guess were supplied to the MATLAB programme. For the solution procedure, the Levenberg-Marquardt algorithm was activated. The stopping criteria for iteration was set at a termination tolerance of 1e-6. A solution was considered achieved when the value of the liquid film thickness was positive and the result of F(x) was very close to zero.

3.5.1. Liquid film thickness

A comparison of experimental liquid film thickness and predictions of the two-fluid model using the selected correlations of interfacial friction factor at liquid viscosity of 100 and 200 mPa respectively as well as v_{sl} of 0.07 m/s respectively is shown in Figure 7.

At liquid At liquid viscosity of 100 mPa s and v_{sl} values of 0.05 m/s and 0.07 m/s,

predictions of the two-fluid using all f_i correlations exhibit the trend of the experimental

Preprints (www.preprints.org) | NOT PEER-REVIEWED | Posted: 6 April 2021 doi:10.20944/preprints202104.0164.v1

data. At v_{sl} of 0.07 m/s, however, it appears predictions of liquid film thickness agree more with the experimental data at low superficial gas velocities. At both v_{sl} and v_{sg} values, the correlations present satisfactory results. The correlations of Belt et al. [19], Ambrosini et al. [17], Wongwises and Kongkiatwanitch [1] and Akagawa et al. [20] present the best performances at both v_{sl} values respectively.

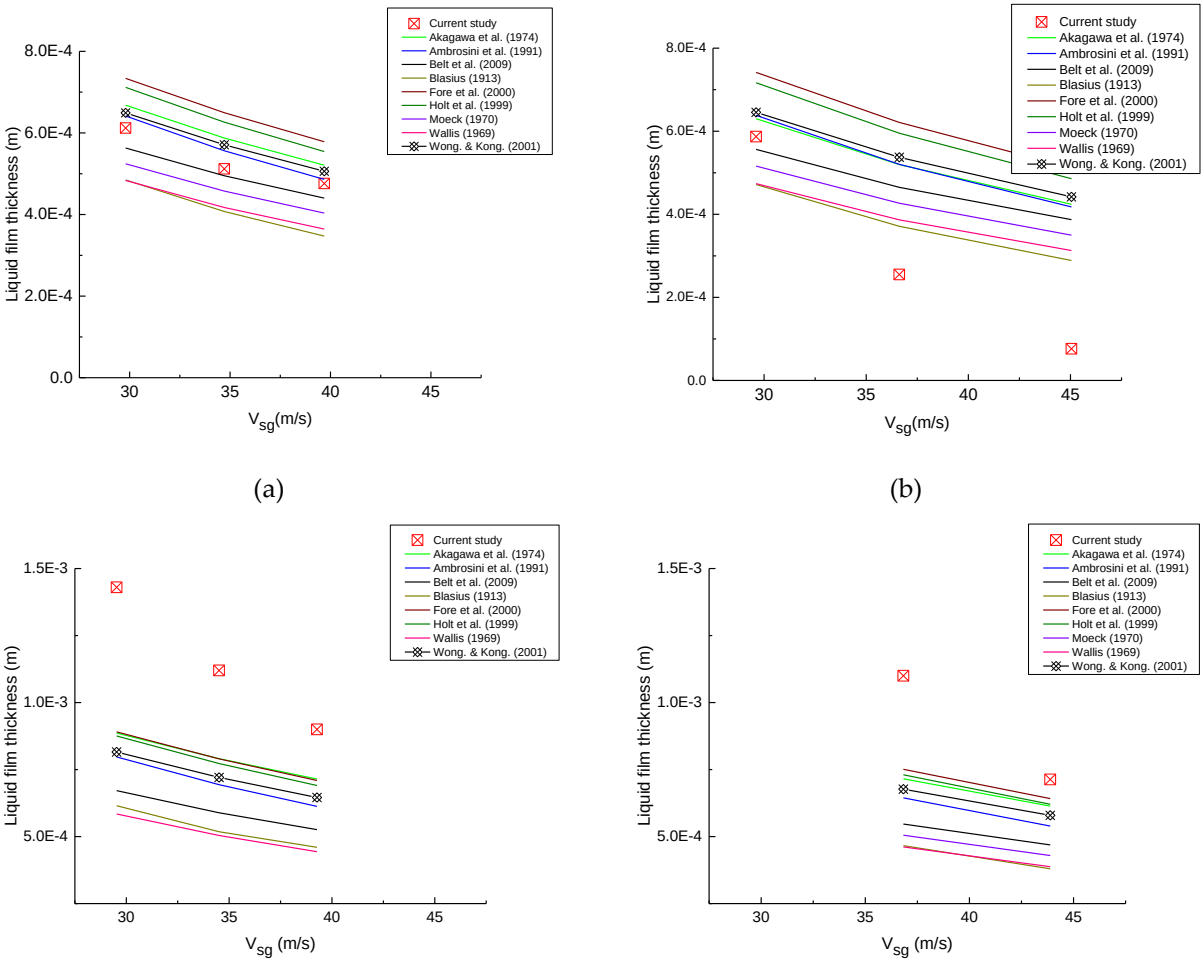

Figure 7 Comparison of experimental liquid film thickness with predictions of two-fluid model using selected

When the liquid viscosity is increased to 200 mPa s (Figure 7), it is found that all predictions by the model underpredict the data at all v_{sl} values. At v_{sl} of 0.05 m/s, the closest predictions are presented (in order of reducing accuracy) by Akagawa et al. [20], Fore et al. [21], Holt et al. [22], Wongwises and Kongkiatwanitch [1] and Ambrosini et al. [17]. When v_{sl} increases to 0.07 m/s, the closest predictions are presented (in order of reducing accuracy) by Fore et al. [21], Holt et al. [22], Akagawa et al. [20], Wongwises and Kongkiatwanitch [1] and Ambrosini et al. [17]. It can be concluded that there is better agreement at liquid viscosity of 100 mPa s than at higher viscosity of 200 mPa s.

3.5.2 Gas void fraction

Preprints (www.preprints.org) | NOT PEER-REVIEWED | Posted: 6 April 2021 doi:10.20944/preprints202104.0164.v1

Figures 8 (a) and (b) show a comparison of the experimental gas void fraction with the predictions of the two- fluid model at a liquid viscosity of 100 mPa s and v_{sl} values of 0.05 and 0.07 m/s respectively. At v_{sl} of 0.05 m/s, the predicted gas void fraction values are comparatively accurate for all f_i correlations utilized. At v_{sl} value of 0.07 m/s, predictions agree better at low values of v_{sg} than at high v_{sg} values. For the case of the liquid viscosity at 200 mPa s, reasonable over-predictions of gas void fraction are observed at both v_{sl} values of 0.05 and 0.07 m/s respectively.

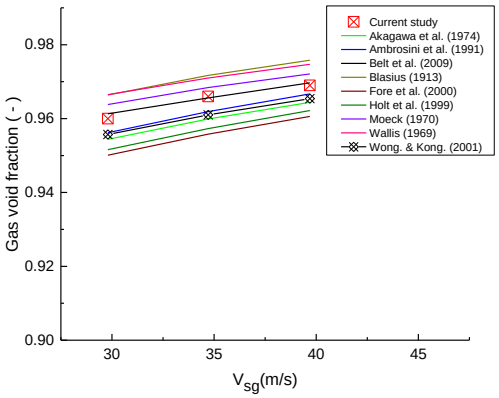

(a)

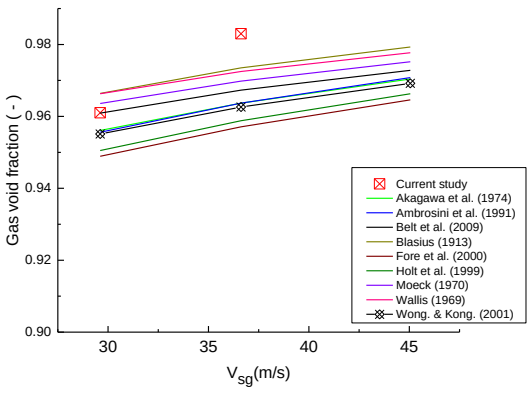

(b)

Preprints (www.preprints.org) | NOT PEER-REVIEWED | Posted: 6 April 2021 doi:10.20944/preprints202104.0164.v1

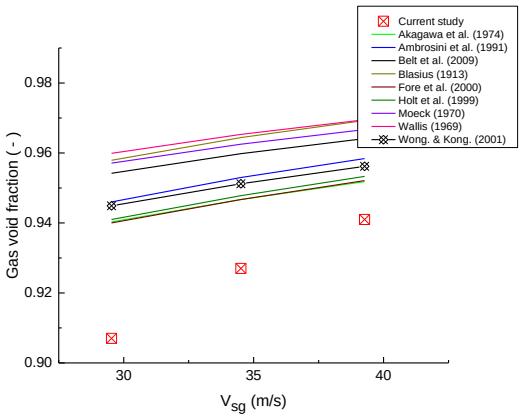

(c)

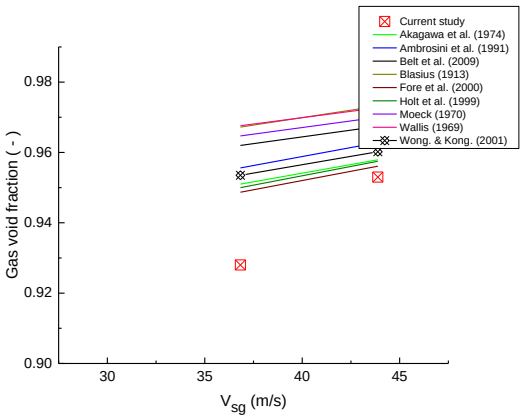

(d)

Figure 8 Comparison of experimental gas void fraction with predictions of two-fluid model using selected f_i correlation at 100 (a),(b) and 200 (c),(d) mPa s

Equation 16 explains the observed characteristics of the predictions in Figures 8 and 9. The equation expresses the mathematical relationship showing that void fraction as a function of superficial gas and liquid velocities as well as accurate predictions of both liquid entrainment fraction and liquid film thickness. In this study, accurate predictions of liquid film thickness become paramount because the other variables can be assumed to be held constant at the specified flow condition. From the Equation, it can be inferred that overprediction of liquid film thickness results in underprediction of values of gas void fraction and vice versa. Significant overprediction is being observed in Figure 9 (a) as a result of underprediction in liquid film entrainment (Figure 8a).

3.5.3 Pressure Gradient

Figure 9 shows the efficiency of pressure gradient predictions from the selected correlations for interfacial friction factor for liquid viscosities of 100 and 200 mPa s respectively. The statistical tools, absolute average percent error (AAPE) and average

Preprints (www.preprints.org) | NOT PEER-REVIEWED | Posted: 6 April 2021 doi:10.20944/preprints202104.0164.v1

percent error (APE) expressed in Equations (20) and (21) were employed to determine the prediction errors.

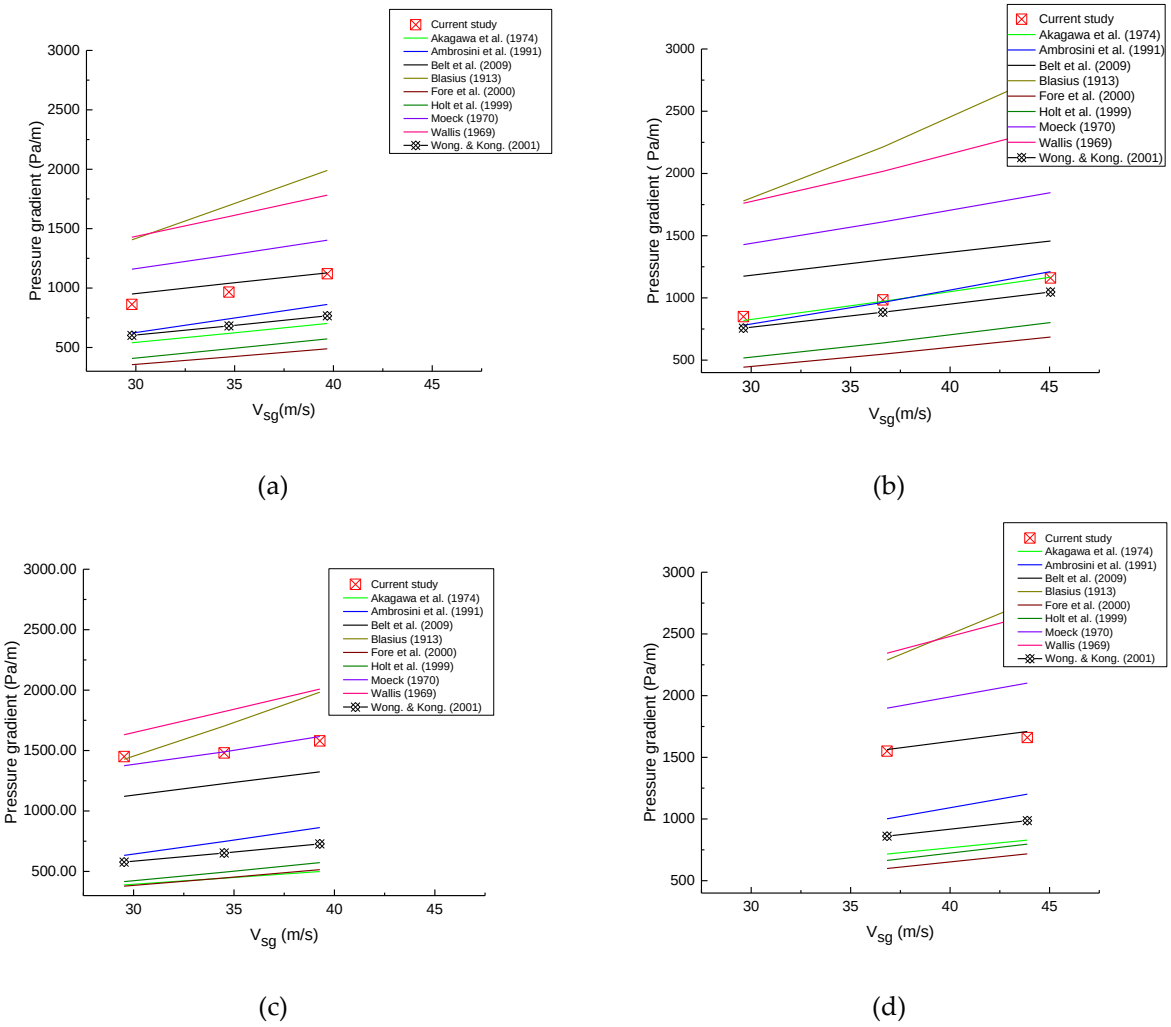

Figure 9 Pressure gradient predictions using selected fi correlations at 100 (a),(b) and 200 (c),(d) mPa s

At a liquid viscosity of 100 mPa s (Figures 9 (a) and (b)), it can be observed that the f_i correlations of both Blasius and Wallis follow the trend of the experimental data but also overpredict the experimental data compared to the correlations. At superficial liquid velocities of 0.05 and 0.07 m/s, predictions of the two- fluid model using the other f_i correlations are satisfactory. Over the entire data for liquid viscosity of 100 mPa s, the four best pressure gradient predictions are achieved using f_i correlations of Ambrosini et al. [17], Akagawa et al. [20], Wongwises and Kongkiatwanitch [1] and Belt et al. [19], listed in order of decreasing accuracy, offer the best pressure gradient predictions.

When the liquid viscosity is increased two-fold (Figures 8 (c) and (d)), the pressure gradient predictions of the obtained using the selected correlations follow the pattern of the experimental data. At v_{sl} of 0.05 m/s, the f_i correlations of Moeck [23], Wallis [14],

Preprints (www.preprints.org) | NOT PEER-REVIEWED | Posted: 6 April 2021 doi:10.20944/preprints202104.0164.v1

Blasius [20] and Fore et al. [21] are observed to give the most accurate predictions. Though the others underpredict the experimental data, their predictions are found to be equally satisfactory. At v_{sl} of 0.07 m/s, the f_i correlations of Wallis and Blasius are observed to slightly overpredict the experimental data. It appears utilization of the Wongwises and Kongkiatwanitch [1] correlation enables the two-fluid model to predict the trend of the data more accurately than the others. Statistical analyses, using AAPE and APE, indicate that the f_i correlations of Belt et al. [19] offers the best predictions over the entire data obtained with liquid viscosity of 200 mPa s followed by that of Moeck and Ambrosini et al. [17] respectively.

Accurate prediction of pressure gradient requires accuracy in the prediction of geometrical parameters as well as the respective velocities of the liquid film and gas core, all of which rely heavily of accurate predictions of the liquid film thickness. As observed from Figure 7, all the correlations appear to predict the gas void fraction fairly accurately. Further, if liquid friction factor and liquid entrainment fraction are assumed fixed for each flow condition, the pressure gradient predictions of the two-fluid model can be viewed as a direct result of the differences in the approach or theory as well as experimental conditions used for for f_i correlation development.

At both viscosities evaluated (100 and 200 mPa s), the correlations of Ambrosini et al. [17] and Belt et al. [19] present good and consistent performances for liquid holdup and pressure gradient predictions. The performance of the Ambrosini et al. [17] correlation could be attributed to the development of the correlation using a wide range of fluid properties. On the other hand, though the Belt et al. [19] correlation was developed based on data obtained with air-water mixtures, its performance could be attributable to fact that the flow conditions agree with their proposed theory which relates the roughness of the liquid film to wave height.

4. Discussion

Authors should discuss the results and how they can be interpreted from the perspective of previous studies and of the working hypotheses. The findings and their implications should be discussed in the broadest context possible. Future research directions may also be highlighted.

5. Conclusions

An experimental investigation of vertical air and oil (with viscosities 100 and 200 mPa s) flow in a 0.060-m ID pipe is reported. Superficial air and oil velocity ranges are from 22.37 to 59.60 m/s and 0.05 to 0.16 m/s respectively. Annular flow pattern at the flow condition considered.

A two-fluid model is developed for prediction of gas void, liquid holdup, and pressure gradient. A combined momentum equation for the gas and liquid phases is developed and solved to generate values of liquid film thickness and subsequently predict the liquid holdup and pressure gradient at given experimental conditions. The influence of accuracy of estimation of interfacial friction factor on accurate determination of the flow characteristics mentioned is investigated by integrating interfacial friction factors from selected correlations.

 doi:10.20944/preprints202104.0164.v1

The results indicate that the two-fluid model is a reliable model capable of predicting accurately upward annular flow characteristics involving high-viscosity liquids including liquid film thickness, gas void fraction and pressure gradient in conduits. Further, the investigation reveals that the best performing correlation are the Belt et al. [19] and Ambrosini et al. [17] correlations. The performance of the Belt et al. [19] equation can possibly be attributed to agreement of the flow conditions with their proposed theory that sand-grain roughness of the liquid film is proportional to wave height while on the other hand, that of Ambrosini et al. [17] can be attributed to the ability of their correlation to accommodate the viscosity differences adequately.

Author Contributions: Conceptualization: Dr. Joseph X. F. Ribeiro and Dr. Aliyu M. Aliyu; Methodology, Dr. Joseph X. F. Ribeiro and Dr. Aliyu M. Aliyu.; Software, Dr. Joseph X. F. Ribeiro and Dr. Aliyu M. Aliyu.; validation, Dr. Joseph X. F. Ribeiro and Dr. Aliyu M. Aliyu.; formal analysis, Dr. Joseph X. F. Ribeiro and Dr. Aliyu M. Aliyu.; investigation, Dr. Joseph X. F. Ribeiro and Dr. Aliyu M. Aliyu; resources, Prof. Ruiquan Liao.; data curation, Dr. Joseph X. F. Ribeiro and Dr. Zilong Liu; writing— Dr. Joseph X. F. Ribeiro; writing—review and editing, Dr. Joseph X. F. Ribeiro Dr. Aliyu M. Aliyu and Dr. Salem Khalifa Brini Ahmed; supervision, Prof. Ruiquan Liao.; project administration, Prof. Ruiquan Liao.; funding acquisition, Prof. Ruiquan Liao. All authors have read and agreed to the published version of the manuscript."

Acknowledgments: This work is supported by National Science and Technology Major Project of the Ministry of Science and Technology of China (2017ZX05030-003-005)

Conflicts of Interest: The authors declare no conflict of interest.

Symbols used

A		area
d, D	[m]	diameter
Fr	[-]	Froude number
f	[-]	friction factor
f_E	[-]	droplet entrainment fraction
g	[m/s²]	gravitational acceleration
H	[-]	Holdup
R_e	[-]	Reynolds number
S	[m]	perimeter
t	[m]	liquid film thickness
v	[m/s]	velocity
$\left(\frac{dp}{dz}\right)$	[Pa/m]	pressure gradient

Greek letters

τ	$[kN/m^2]$	shear stress

Preprints (www.preprints.org) | NOT PEER-REVIEWED | Posted: 6 April 2021 doi:10.20944/preprints202104.0164.v1

δ_l	[m]	liquid film thickness
ρ	[kg/m^3]	density
θ	[°]	angle of inclination
α	[-]	gas void fraction
μ	[mPa s]	viscosity
σ	surface tension	

Subscripts

C	Core
F	Film
wL	wall – liquid interface
i	interfacial
l	liquid
sl	superficial liquid
sg	superficial gas

References

[1] S. Wongwises and W. Kongkiatwanitch, *Int. Commun. Heat Mass Transf.*, 28 (3), 323–336, 2001. DOI:https://doi.org/10.5923/j.jmea.20170705.08

[2] I. M. Alves, E. F. Caetano, K. Minami, and O. Shoham, *SPE Prod. Eng.*, 6 (4), 435–440, 1991. DOI:https://doi.org/10.2118/20384-PA

[3] R. V. A. Oliemans, B. F. M. Pots, and N. Trompé, *Int. J. Multiph. Flow*, 12 (5), 711–732, 1986. DOI:https://doi.org/10.1016/0301-9322(86)90047-9

[4] M. B. Alamu, "Investigation of periodic structures in gas-liquid flow, Ph.D. thesis," University of Nottingham, 2010.

[5] R. E. Vieira *et al.*, *Exp. Therm. Fluid Sci.*, 64, 81–93, 2015. DOI:https://doi.org/10.1016/j.ces.2015.03.033

[6] H.-Q. Zhang, Q. Wang, C. Sarica, and J. P. Brill, *J. Energy Resour. Technol.*, 125 (4), 266-273, 2003. DOI:https://doi.org/10.1115/1.1615246

[7] K. Aziz and G. W. Govier, *J. Can. Pet. Technol.*, 11 (3), 38–48, 1972. DOI:https:// doi.org/10.2118/72-03-04

[8] A. Hagedorn and K. Brown, *J. Pet. Technol.*, 16 (2), 203–210, 1964. DOI:https:// doi.org/10.2118/733-PA

[9] H. Duns and N. C. J. Ros, *6th World Pet. Congr.*, 451–465, 1963.

[10] H. Mukherjee and J. P. Brill, *J. Energy Resour. Technol.*, 107 (4), 549-554, 1985. DOI:https:// doi.org/

10.1115/1.3231233

[11] D. H. Beggs and J. P. Brill, *J. Pet. Technol.*, 25 (5), 607–617, 1973. DOI:https:// doi.org/10.1115/1.3231233

[12] Orkiszewski, J., *J. Pet. Technol.*, 19 (6), 829–838., 1967. DOI:https://doi.org/10.2118/1546-PA

[13] D. A. McNeil and A. D. Stuart, *Int. J. Multiph. Flow*, 29, 9, 1523–1549, 2003. DOI:https://doi.org/ 10.1016/S0301-9322(03)00122-8

[14] G. B. Wallis, *One-Dimensional Two-phase Flow*. McGraw Hill, New York, 1969.

[15] P. Sawant, M. Ishii, and M. Mori, *Int. J. Heat Fluid Flow*, 30 (4), 715–728, 2009. DOI:https:// doi.org/10.1016/j.ijheatfluidflow.2009.03.003

[16] A. M. Aliyu, Y. D. Baba, L. Lao, H. Yeung and K. C. Kim, *Exp. Therm. Fluid Sci.*, 85, 287–304, 2017. DOI:https://doi.org/10.1016/j.expthermflusci.2017.02.006

[17] W. Ambrosini, P. Andreussi, and B. J. Azzopardi, *Int. J. Multiph. Flow*, 17 (4), 497–507, 1991. DOI:https://doi.org/10.1016/0301-9322(91)90045-5

[18] F. Matsuyama, M. Sadatomi, K. Nakashima, Y. Johno, and T. Shigematsu, *J. Mech. Eng. Autom.*, 7, 1–8, 2013. DOI:https://doi.org/10.5923/j.jmea.20170705.08

[19] R. J. Belt, J. M. C. Van't Westende, and L. M. Portela, *Int. J. Multiph. Flow*, 35 (7), 689–697, 2009. DOI:https://doi.org/10.1016/j.ijmultiphaseflow.2008.12.003

[20] A. M. Aliyu, Y. D. Baba, L. Lao, H. Yeung, and K. C. Kim, *Exp. Therm. Fluid Sci.*, 84, 90–109, 2017. DOI:https://doi.org/10.1016/j.expthermflusci.2017.02.006

[21] L. B. Fore, S. G. Beus, and R. C. Bauer, *Int. J. Multiph. Flow*, 26 (11), 1755–1769, 2000. DOI:https:// doi.org/doi.org/10.1016/S0301-9322(99)00114-7

[22] A. J. Holt, B. J. Azzopardi, and M. W. Biddulph, *Chem. Eng. Res. Des.*, 77 (1), 7–15, 1999. DOI:https://doi.org/10.1205/026387699525828

[23] E. O. Moeck, Annular - dispersed two-phase flow and critical heat flux,1970.

[24] T. Fukano and T. Furukawa, *Int. J. Multiph. Flow*, 24 (4), 587–603, 1998.

[25] J. C. Asali, T. J. Hanratty, and P. Andreussi, *AIChE J.*, 31 (6), 895–902, 1985. DOI:https://doi.org/ 10.1002/aic.690310604

[26] L. B. Fore and A. E. Dukler, *AIChE J.*, 41 (9), 2040–2046, 1995. DOI:https://doi.org/ 10.1002/aic.690410904

[27] M. . H. S. Zangana, Film behaviour of vertical gas-liquid flow in a large diameter pipe,Ph.D thesis,University of Nottingham, 2011.

[28] A. Skopich, E. Pereyra, C. Sarica, and M. Kelkar, "*SPE Prod. Oper.*, 30 (2), 164–176, 2015. DOI:https:// doi.org/10.2118/164477-PA

[29] G. P. Van der Meulen, Churn-annular gas-liquid flows in large diameter vertical pipes, Ph.D thesis, University of Nottingham, 2012.

[30] C. J. Shearer and R. M. Nedderman, *Chem. Eng. Sci.*, 20 (7), 671–683, 1965. DOI:https:// doi.org/ 10.1016/0009-2509(65)80004-5

[31] N. P. del Corral, Analysis of Two-Phase Flow Pattern Maps, 2014.

[32] Y. Taitel, D. Bornea, and A. E. Dukler, *AIChE J.*, 26 (3), 345–354, 1980. DOI:https://doi.org/ 10.1002/aic.690260304

[33] F. Al-Ruhaimani, E. Pereyra, C. Sarica, E. M. Al-Safran, and C. F. Torres, *SPE J.*, 22 (3), 0712–0735, 2017. DOI:https://doi.org/10.2118/184401-PA

[34] F. Matsuyama, M. Sadatomi, K. Nakashima, and Y. Johno, *J. Mech. Eng. Autom.*, 7 (5), 164–171, 2017. DOI:https://doi.org/10.5923/j.jmea.20170705.08

[35] R. Kaji and B. J. Azzopardi, *Int. J. Multiph. Flow*, 36 (4), 303–313, 2010. DOI:https://doi.org/10.1016/j.ijmultiphaseflow.2009.11.010

 doi:10.20944/preprints202104.0164.v1